Externally Forced and Internally Generated Decadal Climate Variability Associated with the Interdecadal Pacific Oscillation

GERALD A. MEEHL AND AIXUE HU

National Center for Atmospheric Research, Boulder, Colorado*

JULIE M. ARBLASTER

National Center for Atmospheric Research, Boulder, Colorado, and CAWCR, Bureau of Meteorology, Melbourne, Australia*

JOHN FASULLO AND KEVIN E. TRENBERTH

National Center for Atmospheric Research, Boulder, Colorado*

(Manuscript received 30 July 2012, in final form 7 February 2013)

ABSTRACT

Globally averaged surface air temperatures in some decades show rapid increases (accelerated warming decades), and in other decades there is no warming trend (hiatus decades). A previous study showed that the net energy imbalance at the top of the atmosphere of about 1 W m^{-2} is associated with greater increases of deep ocean heat content below 750 m during the hiatus decades, while there is little globally averaged surface temperature increase or warming in the upper ocean layers. Here the authors examine processes involved with accelerated warming decades and address the relative roles of external forcing from increasing greenhouse gases and internally generated decadal climate variability associated with interdecadal Pacific oscillation (IPO). Model results from the Community Climate System Model, version 4 (CCSM4), show that accelerated warming decades are characterized by rapid warming of globally averaged surface air temperature, greater increases of heat content in the upper ocean layers, and less heat content increase in the deep ocean, opposite to the hiatus decades. In addition to contributions from processes potentially linked to Antarctic Bottom Water (AABW) formation and the Atlantic meridional overturning circulation (AMOC), the positive phase of the IPO, adding to the response to external forcing, is usually associated with accelerated warming decades. Conversely, hiatus decades typically occur with the negative phase of the IPO, when warming from the external forcing is overwhelmed by internally generated cooling in the tropical Pacific. Internally generated hiatus periods of up to 15 years with zero global warming trend are present in the future climate simulations. This suggests that there is a chance that the current observed hiatus could extend for several more years.

1. Introduction

Previous studies have noted that during the first decade of the twenty-first century, globally averaged surface air temperatures showed a near-zero warming trend—termed a hiatus decade (Easterling and Wehner 2009; Katsman and van Oldenborgh 2011; Meehl et al. 2011). However, there has been an ongoing net energy imbalance at the top of the atmosphere of about 0.5–1 W m^{-2} (Hansen et al. 2005; Trenberth 2009), and the speculation is that this energy is likely going into the deep ocean where there are few measurements for verification (Trenberth 2009; Trenberth et al. 2009; Trenberth and Fasullo 2010; Loeb et al. 2012). Observational datasets derived from the Argo float data and other sources indicate a slowing of the rate of ocean heat content above about 700 m during the early 2000s when there was little trend in globally averaged surface temperatures (Levitus et al. 2009, 2012; Lyman et al. 2010). Such hiatus periods with little or no surface warming

* The National Center for Atmospheric Research is sponsored by the National Science Foundation.

Corresponding author address: Gerald Meehl, CCR, CGD/NCAR, P.O. Box 3000, Boulder, CO 80307-3000.
E-mail: meehl@ncar.ucar.edu

DOI: 10.1175/JCLI-D-12-00548.1

trend are relatively common occurrences in observations and in climate model simulations (Easterling and Wehner 2009; Knight et al. 2009; Santer et al. 2011; Katsman and van Oldenborgh 2011; Meehl et al. 2011). Suggestions that significant heat could be sequestered in the subsurface ocean on decadal time scales (e.g., Purkey and Johnson 2010; Song and Colberg 2011; Palmer et al. 2011; Levitus et al. 2012; Guemas et al. 2013; Watanabe et al. 2013; Balmaseda et al. 2013) are consistent with an analysis of a global coupled climate model, which showed that, during hiatus decades in the model, the deep ocean layers did indeed warm at a greater rate than the surface layers (Meehl et al. 2011). That study went on to identify three processes that could contribute to the deep ocean heat content increases during hiatus decades, two having to do with reduced deep ocean mixing associated with a weakening of the Atlantic meridional overturning circulation (AMOC) and reduced Antarctic Bottom Water (AABW) formation and one having to do with an internally generated mode of decadal variability in the Pacific basin called the interdecadal Pacific oscillation (IPO) in its negative phase when tropical Pacific SSTs are below normal (Power et al. 1999; Meehl and Hu 2006; Meehl et al. 2010; Dai 2013; Meehl and Arblaster 2011, 2012).

While Katsman and van Oldenborgh (2011) suggested a role for variability in the planetary imbalance in the context of present-day variability, the relative importance of forced variations (e.g., solar variability, volcanoes, and anthropogenic aerosols) versus internal variability was not quantified. In contrast, here, as in Meehl et al. (2011), our focus is on simulations in which decadal variability is driven largely by internal variations, rather than the rapid changes in forcing that were implicit in the Katsman and van Oldenborgh study. Another single model analysis (Palmer et al. 2011) showed that decadal trends in SST in a preindustrial control run are only weakly indicative of the changes in the planetary imbalance that govern ocean heat content, echoing the main conclusions of the present paper elaborated on below. While it is unclear how the variability in ocean uptake during the transient adjustment of the system to forcing is related to variability in the equilibrium run analyzed by Palmer et al., differences between the Community Climate System Model, version 4 (CCSM4), analyzed here, and the Met Office model, assessed in Palmer et al. (2011), may also explain what seems to be a minor discrepancy of a weak (rather than insignificant) role for top-of-atmosphere (TOA) radiation variations.

The Meehl et al. (2011) study raised several questions that we address here. First, what is happening during decades that are opposite to the hiatus decades, when globally averaged surface air temperatures rapidly warm? Second, there appears to be a large internally generated component to the hiatus decades, but this variability is occurring while increasing greenhouse gases (GHGs) should make the system want to warm. What is the nature of the interplay between the external forcing and the internally generated decadal time scale variability that could produce hiatus decades and accelerated warming decades? A previous study showed that the most notable accelerated warming decade in the twentieth century, the so-called mid-1970s climate shift (Trenberth and Hurrell 1994; Wang and An 2001), was a product of a warming contribution from the increase of GHGs added to warming of the tropical Pacific from a positive phase of the IPO (Meehl et al. 2009). Meanwhile, the transition of the IPO from positive to negative phase in the late 1990s (Chen et al. 2008; Burgman et al. 2008; Feng et al. 2010; Dai 2013; Meehl and Arblaster 2012) was associated with a hiatus of global warming (Meehl et al. 2011). It is this interaction of externally forced response and internally generated decadal time scale variability in the Pacific that we examine in this paper to study the relative contributions to both hiatus and accelerated warming decades. Understanding these processes has important implications for prediction since such decades with either rapid climate change or little climate change would be of interest to the community of users of such decadal climate information.

Section 2 describes the model, experiments, and methodology utilized in the paper. Section 3 contrasts the signatures of surface climate during hiatus and accelerated warming decades in the model, documents the vertical distribution of heating in the ocean, and discusses the processes involved. Section 4 includes an analysis of the relative contributions of external forcing and internally generated time scale variability associated with the IPO in producing hiatus and accelerated warming decades, and section 5 contains the conclusions.

2. The model and experiments

The Community Climate System Model, version 4 is the climate model analyzed here. It is a global coupled climate model with a 1°, 26-level atmosphere coupled to a 1° (down to ¼° in the equatorial tropics), 60-level ocean and state-of-the-art sea ice and land surface schemes (Gent et al. 2011). The CCSM4 response to future increases of GHGs, including the four representative concentration pathway (RCP) mitigation scenarios, is described by Meehl et al. (2012). Five ensemble members from the RCP4.5 simulations with CCSM4 are extended from five corresponding twentieth-century simulations and are analyzed to study hiatus and accelerated warming decades. The CCSM4 is well balanced in the control run such that the net TOA energy flux is

$O(0.1\,\mathrm{W\,m^{-2}})$. We choose to analyze results from the RCP4.5 scenario because it has CO_2 increasing at a rate moderate enough that internally generated decadal time scale variability can occasionally offset the forced warming and produce decades when the surface temperature trend is slightly negative. There are also decades when there is accelerated warming much greater than the long-term trend. We examine a future climate scenario rather than twentieth-century simulations because the latter have combinations of natural and anthropogenic forcings leading to periods of little warming in certain time periods during the first part of the century (e.g., Meehl et al. 2004, 2012). In contrast, future climate simulations offer more realizations of internally generated hiatus and accelerated warming decades in the context of persistently positive anthropogenic forcing from increasing GHGs.

As will be shown below, the net energy flux at the top of the atmosphere during all decades in the RCP4.5 simulations (including hiatus decades, accelerated warming decades, and all other decades) is about $1\,\mathrm{W\,m^{-2}}$, indicative of a net energy surplus being trapped in the climate system. This arises mainly from forced decreases in outgoing longwave radiation from the increases of GHGs, in conjunction with water vapor feedback, not allowing as much energy to escape the climate system, while cloud feedbacks amplify the warming (e.g., Trenberth and Fasullo 2009). The forced energy imbalance includes effects from increased longwave radiation from higher temperatures. Consequently, if there are time periods when surface temperatures are not increasing, this excess energy must go elsewhere. Changes to the cryosphere and land subsurface play a much smaller role than the atmosphere and oceans in energy flows (Trenberth and Fasullo 2010), and the potential importance of the deep ocean in increasing heat content during hiatus decades was shown by Meehl et al. (2011).

In terms of a computational detail, for the ocean meridional overturning streamfunction calculation for the Pacific basin north of about 30°S, we subtract the Indonesian Throughflow (12.6 Sv in CCSM4) ($\mathrm{Sv} \equiv 10^6\,\mathrm{m^3\,s^{-1}}$) from the Pacific basin calculation and add that value to the Indian basin.

3. Results

The hiatus decades were chosen by Meehl et al. (2011) as decades with a linear trend of less than −0.08°C over a decade. Even more decades could have been selected if the criteria would have been a zero trend over a decade, but we chose decades with slightly negative trends to provide larger signals. Thus, eight such decades from the five ensemble members (eight decades out of 500 years of simulation, averaging one every 60 yr or so) are composited and their linear trends of surface air temperature are shown in Fig. 1a.

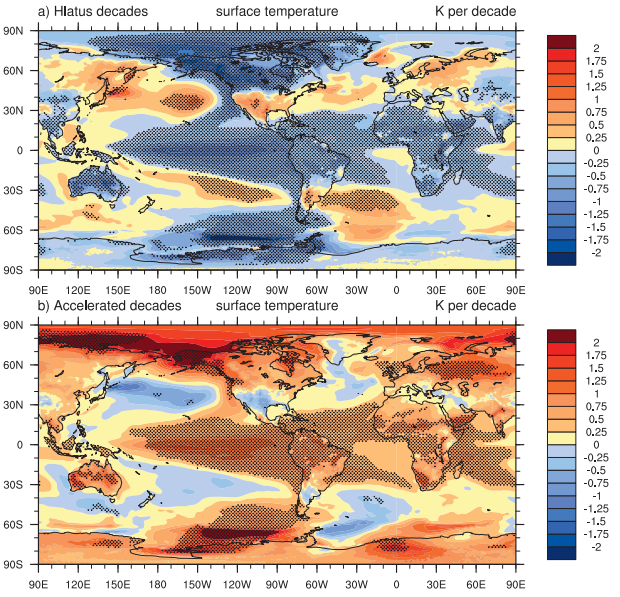

FIG. 1. (a) Composite average SST linear trends ($\mathrm{K\,decade^{-1}}$) for decades when there is a hiatus of global warming as defined in the text: stippling indicates 5% significance computed from a two-sided t test. (b) As in (a) but for accelerated warming decades.

If a criterion of zero trend in globally averaged surface air temperatures is applied, similar to what has recently been observed, there are 14 such decades in the RCP4.5 simulations [taking only time periods prior to 2080 after which the forcing and corresponding temperature response has lower magnitude (Meehl et al. 2012), thus using 375 years of model simulations]. Additionally, using that same criterion and time periods in the five RCP4.5 ensemble members, there are nine instances of 11-yr zero temperature trends, six instances of 12-yr zero temperature trends, five instances of 13-yr zero temperature trends, three instances of 14-yr zero temperature trends, and one instance of a 15-yr zero temperature trend. Thus, the occurrence of a 15-yr duration, internally generated zero temperature trend, though rare in the model (one event in 375 years of model simulations), suggests that there is a chance the current observed hiatus could continue for several more years.

Meanwhile, seven accelerated warming decades are chosen from the five ensemble members of RCP4.5 (seven decades out of 475 years of simulation, averaging one every 70 yr or so) based on the criterion of a globally averaged surface air temperature trend of greater than or equal to 0.41 $\mathrm{K\,decade^{-1}}$ (a relatively large threshold to isolate on the largest signals). The composites of the linear trends of SST from those accelerated warming

decades are shown in Fig. 1b. Statistical significance is computed from a two-sided Student's t test (since we have no expectation of the sign of the SST trend change) of the hiatus or accelerated trends compared to 435 possible decadal trends across the five ensemble members with an equivalent sample size, taking into account autocorrelation, of 45 degrees of freedom. Similar values are returned both when including and excluding the hiatus and accelerated trend periods in the larger sample. This methodology is applied to all t-test calculations in this paper. With regards to the SST patterns in Fig. 1, visual inspection of the actual SST anomaly patterns of the hiatus and accelerated warming periods confirms the results of this test in that each hiatus period is characterized in a recognizable way as a negative IPO pattern and, likewise, for each accelerated warming period as a positive IPO pattern.

What is immediately striking about the comparison of Figs. 1a and 1b is that the patterns are nearly mirror images of each other, with the signature of a negative (positive) phase of the IPO in the Pacific in the hiatus (accelerated warming) decades and the phase of the IPO indicating the relative sign of the SST trends in the tropical Pacific. The sign of the SST trends for both hiatus and accelerated warming decades extends to the Atlantic and Indian Oceans as well, with opposite sign trends in the northwest and southwest Pacific and North Atlantic.

The composite SST trend decades have a similar energy imbalance at the top of the atmosphere, with the hiatus decades (Fig. 2, top) and accelerated warming decades (Fig. 2, bottom) showing an imbalance of about $1\,\mathrm{W\,m^{-2}}$, comparable to the imbalance for all other decades with no significant difference between them. Therefore, in all decades there is about $1\,\mathrm{W\,m^{-2}}$ being directed into the climate system, and the planet is warming. If all of the heat from this energy imbalance were directed into the oceans, this would amount to about $16.09 \times 10^{22}\,\mathrm{J\,decade^{-1}}$.

To identify the associated distribution of heat content trends in the ocean for hiatus and accelerated warming decades, Fig. 2 shows globally averaged 10-yr ocean heat content trends for three layers in the global ocean, the upper 300, 300–750, and 750 m to the bottom of the ocean for hiatus (Fig. 2, top) and accelerated warming decades (Fig. 2, bottom). The 750-m level was chosen for reasons of historical observations.

Nonoverlapping error bars in Fig. 2, defined as ±1.86 standard error, are used to show statistical significance at the 5% level, as in Meehl et al. (2011). Nonoverlapping error bars imply rejection of the null hypothesis in the one-sided formal t test in addition to the formal t test based on the difference between two means. To demonstrate this, we define X_2 and X_1 as the two mean

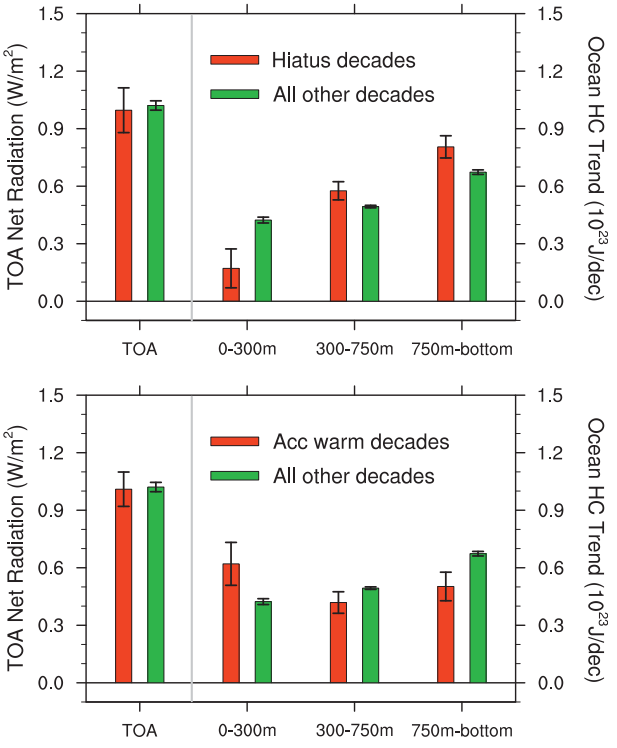

FIG. 2. (top) Composite mean global linear trends for decades when there is a hiatus of global warming, as defined in the text (red bars), and mean linear trends for all other decades (green bars) for TOA net radiation at left ($\mathrm{W\,m^{-2}}$, positive values denote net energy entering the system). The right part of the figure depicts decadal trends of global ocean heat content ($10^{23}\,\mathrm{J\,decade^{-1}}$) for the upper ocean (surface to 300 m) and two deeper ocean layers (300–750 and 750–3000 m) for the composite hiatus decades (red bars) and average for all other decades (green bars); error bars denote 5% significance. (bottom) As in (top) but for accelerated warming decades.

quantities computed from the two sets of $n = 5$ ensemble members. Standard error is defined as

$$S_1 \equiv \sqrt{S_1^2} = \sqrt{\frac{\sum (X_{1i} - X_1)^2}{n-1}},$$

where i runs from 1 to n, and S_2 is similarly defined.

For the case when $X_2 > X_1$, consistent with expectations of a warmer ocean and, thus, the use of the one-sided t test, X_2 and X_1 are significantly different because, by applying the nonoverlapping error bar criterion,

$$X_2 - 1.86S_2 > X_1 + 1.86S_1.$$

That can be written as

$$X_2 - X_1 > 1.86(S_1 + S_2). \quad (1)$$

By the definition of S_1 and S_2, since

$$S_1 + S_2 \geq \sqrt{S_1^2 + S_2^2},$$

Eq. (1) therefore implies

$$X_2 - X_1 \geq 1.86\sqrt{S_1^2 + S_2^2},$$

which indicates rejection of the null hypothesis in a one-sided t test at the 5% level since the 95% quantile of a Student's t test with eight degrees of freedom for the hiatus decades is 1.86. For the accelerated warming decades, this value is 1.89.

As for the SST trends in Fig. 1, the hiatus decades and accelerated warming decades show nearly opposite results, as noted above. The upper 300-m layer has a significantly lower magnitude heat content trend (no overlap of the error bars indicating significance at the 5% level), with a value of $+1.7 \times 10^{22}$ J decade^{-1}, a reduction of 60% compared to the average trend over all 10-yr time periods for the five ensemble members of $+4.2 \times 10^{22}$ J decade^{-1}.

However, in the deeper layers of the global ocean for hiatus decades in Fig. 2 (top), the heat content trends are greater than in other decades. For the 300–750-m layer, the composite global average is 18% larger [+5.8 versus +4.9 ($\times 10^{22}$ J decade^{-1})] and, for the layer below 750 m, the composite global average is 19% larger ($+8.0 \times 10^{22}$ compared to $+6.7 \times 10^{22}$ J decade^{-1}). The error bar ranges do not overlap for either layer, again indicating these differences are statistically significant at the 5% level.

However, for the accelerated warming decades in Fig. 2 (bottom), the heat content trends are opposite to those for the hiatus decades in Fig. 2 (top). Where there was a reduction in upper ocean layer heat content trends in the hiatus decades in Fig. 2 (top), there is a statistically significant increase in heat content trend in the upper 300-m layer of $+7.0 \times 10^{22}$ J decade^{-1} for accelerated warming decades. This is an increase of 56% compared to $+4.5 \times 10^{22}$ J decade^{-1} for all other decades. Meanwhile, there is a statistically significant reduction of heat content trends in the deeper ocean layers in accelerated warming decades (Fig. 2, bottom) compared to increased heat content trends in those layers for the hiatus decades (Fig. 2, top). For the 300–750-m layer, accelerated warming decade heat content trends are reduced 16% from $+5.0 \times 10^{22}$ for all decades to $+4.2 \times 10^{22}$ J decade^{-1} for accelerated warming decades. Similarly for the deepest layer from 750 m to the ocean bottom, the accelerated warming decade trend is $+5.0 \times 10^{22}$ compared to $+6.8 \times 10^{22}$ J decade^{-1} for all other decades, a reduction of 26%.

A breakdown of ocean heat content trends by basin (shown for the hiatus decades by Meehl et al. 2011) indicates similar outcomes for the accelerated warming decades (not shown) to the global numbers shown in Fig. 2, with opposite trend differences to the hiatus decades. Thus, for the accelerated warming decades, there are greater heat content trends in the surface layers compared to all other decades and significantly reduced heat content trends in the deepest layers in all basins, with the largest reduction of 25% in the Southern Ocean, suggestive of an increase of AABW formation in accelerated warming decades. There is also a reduction of 15% in the Atlantic, indicative of an increased North Atlantic Deep Water (NADW) formation, and a stronger AMOC there, as discussed further below.

The long-term climatological average of annual-mean ocean meridional overturning streamfunction in the CCSM4 is shown in Figs. 3a and 3b, where positive streamfunction contours indicate clockwise flow and negative streamfunction contours are counterclockwise. The subtropical cells (STCs), which are dominant mainly in the Pacific (e.g., Klinger and Marotzke 2000; McPhaden and Zhang 2002, 2004), are shown by the largest opposite-sign streamfunction values above about 700 m between roughly 35°N and 35°S with upward flow near the equator and convergence and downward flow near 35°N; the AMOC is represented as greatest positive values near 40°N at 1000 m depth and sinking north of about 45°N. The Ekman divergence in the Southern Ocean near 60°S is shown by maximum positive values centered near 50°S, while the AABW formation is indicated by negative values poleward of about 65°S and negative values below ~3000 m that extend into the Northern Hemisphere.

Composite trends for the hiatus and accelerated warming decadal trends for meridional overturning streamfunction averaged over the Pacific basin for the layer above ~700 m (Figs. 3c,d; note the difference in vertical scale compared to Figs. 3a,b) show opposite-sign trend anomalies between hiatus and accelerated warming decades. Positive trend values from about the equator to 40°N, and mostly negative values from the equator to ~35°S in the hiatus decades in Fig. 3c, indicate an anomalous strengthening of the STCs in the Pacific (McPhaden and Zhang 2004), while anomalies of opposite sign for the accelerated warming decades show a weakening of the STCs (McPhaden and Zhang 2002) in Fig. 3d. For the hiatus decades, this produces stronger upward vertical motion near the equator, bringing more cool water to the surface there and negative decadal temperature trends in the equatorial Pacific (Fig. 1a), while weaker STCs in the accelerated warming decades produce the opposite effect. For the hiatus decades, greater convergence near the subtropics of each hemisphere downwells warm water (e.g., positive decadal temperature trends from about 30° to 45°N and south of 30°S in Fig. 3e), while weaker STCs in the accelerated warming decades reduce downwelling, producing cooling

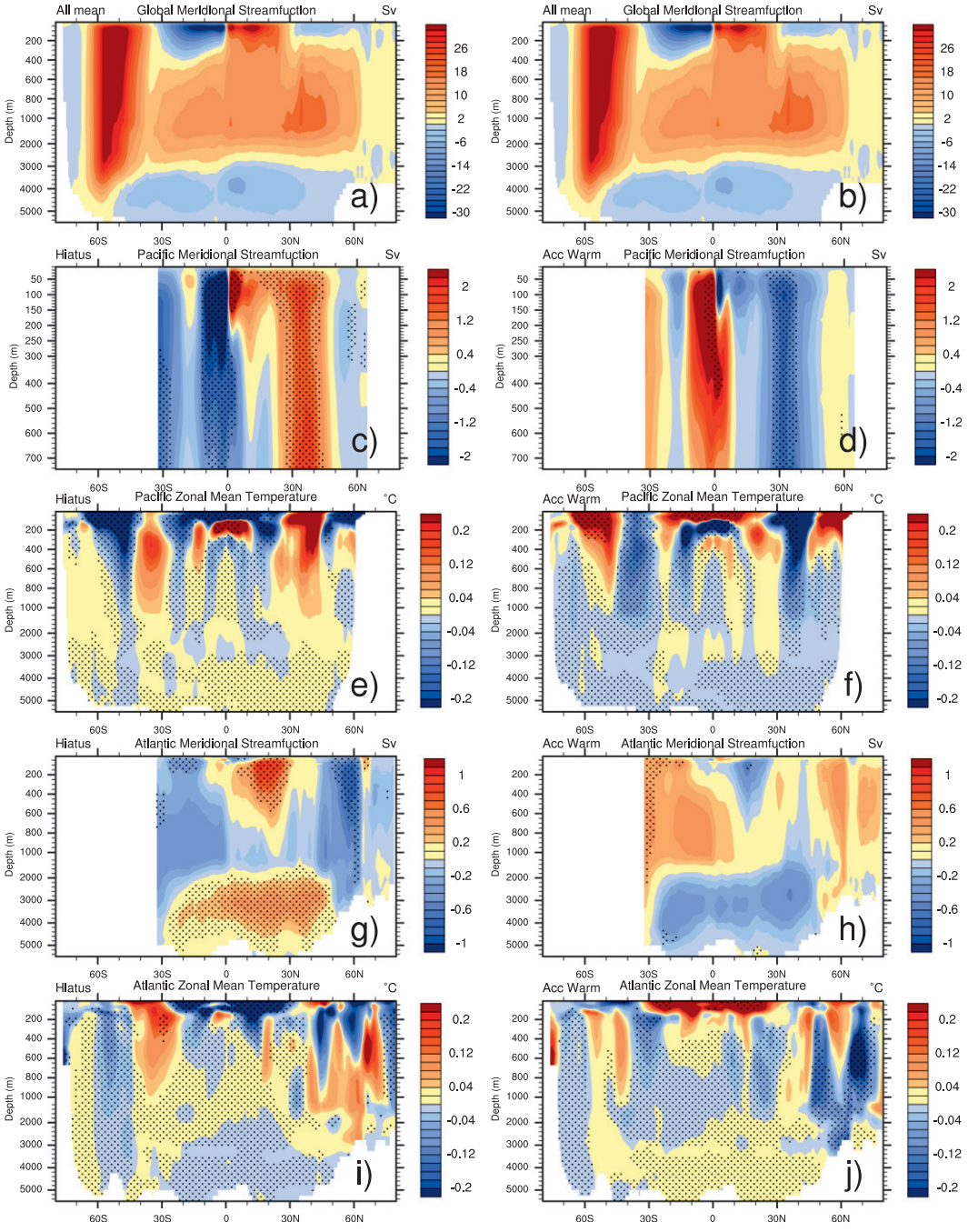

FIG. 3. (a),(b) Zonal mean long-term average global ocean meridional overturning streamfunction (Sv) from CCSM4. Composite linear trend anomalies for (c) hiatus decades and (d) accelerated warming decades relative to the ensemble mean linear trends of other decades for meridional overturning streamfunction (Sv decade^{-1}) for the upper Pacific Ocean (note different vertical scale from (a). (e),(f) As in (c),(d) but for zonal mean temperature (°C decade^{-1}) for the Pacific Ocean. Meridional overturning streamfunction trends (Sv decade^{-1}) for the Atlantic Ocean for (g) hiatus decades and (h) accelerated warming decades. (i),(j) As in (e),(f) but for the Atlantic. Stippling in all panels indicates 5% significance computed from a two-sided t test.

to 2000 m (Fig. 3f). For the hiatus decades, there is mostly small amplitude warming south of 60°S, spreading equatorward at depth (Fig. 3e), suggestive of a weakening of AABW formation. The accelerated warming decades (Fig. 3f) show the opposite, with negative temperature trends south of 60°S and at depth, spreading equatorward, indicative of stronger AABW formation.

In the North Atlantic for the hiatus decades, the composite streamfunction (Fig. 3g) shows a mostly negative trend, implying a weakening of the deep convection with less subduction of cold surface waters, indirectly inducing a warming effect in the subsurface and deep ocean in the Atlantic (Brady and Otto-Bliesner 2011). For the accelerated warming decades there is an opposite sign of the streamfunction anomalies (Fig. 3h), suggestive of a stronger AMOC, as evidenced by negative temperature trends down to about 3000 m (Fig. 3j). The negative zonal mean temperature trends south of 60°S and at depth (Fig. 3j) are again indicative of a possible strengthening of AABW formation.

Though the composites show the net contributions from the three processes noted above (AABW formation, AMOC, and STCs associated with the IPO), examination of each of the hiatus and accelerated warming decades shows contributions from each process. For example, the hiatus decades show that three of those decades have contributions from all three processes, three have more dominant contributions from two of the three, and two have a stronger contribution from one of the processes. The accelerated warming decades are comparable with one of those decades having contributions from all three processes, one decade has a stronger contribution from two out of three, and five have one out of three. However, of the three processes, the STCs associated with the IPO have the most consistent contribution to the hiatus and accelerated warming decades.

Figure 4 shows differences in mixed layer depth (meters) for composite hiatus minus accelerated warming decades for high latitudes of the Northern and Southern Hemispheres. Negative differences in the Labrador Sea in March (Fig. 4, top) and in the Weddell Sea in September (Fig. 4, bottom) indicate shallower mixed layer depth maxima, indicative of reduced deep convection and weakened AMOC and AABW formation in those locations for hiatus decades: the opposite occurs for accelerated warming decades, consistent with the temperature differences discussed above in Fig. 3.

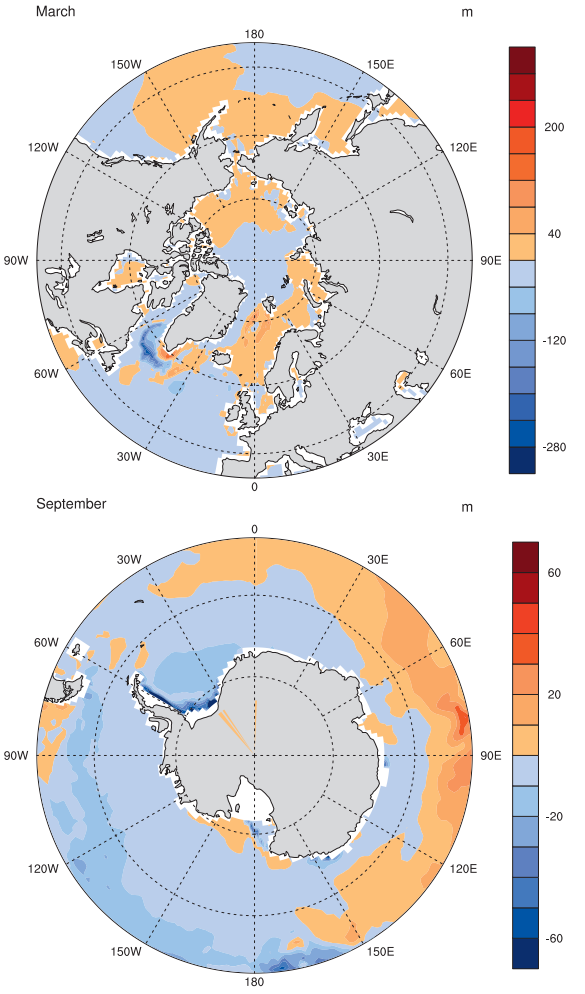

FIG. 4. Differences in maximum mixed layer depth (m) for composite hiatus minus accelerated warming decades for high latitudes of the (top) Northern and (bottom) Southern Hemispheres. Negative differences in the Labrador Sea in March and in the Weddell Sea in September indicate weakened AMOC and AABW formation in those locations.

4. External forcing and internally generated variability

The external forcing from increasing GHGs is positive throughout the model simulations and could be expected to produce mostly warming of the global climate system (Meehl et al. 2012). However, the interaction of the response to this external forcing with internally generated variability is particularly evident in the manifestation of regional patterns of surface temperature change in the Pacific. For example, Meehl et al. (2009) addressed the relative contributions of external forcing mainly from increasing GHGs and internally generated variability from the IPO in the mid-1970s climate shift. They noted that the SST pattern from the internally generated IPO, quantified from a long unforced control run with the Parallel Climate Model (PCM) as the first EOF of low-pass filtered SSTs, was not independent from the SST pattern from external forcing (quantified as the second EOF of an ensemble average of twentieth-century

all-forcings simulations). Thus, they inferred relative contributions using a regression-based technique and determined that the mid-1970s shift had about equal contributions from the tropical Pacific warming attributed to the IPO transitioning on its own from a negative to positive phase, combined with the warming from increasing GHGs. That example was an attempt to explain an observed accelerated warming period.

Though it was discussed in Fig. 3 (and by Meehl et al. 2011) that at least three sets of regional processes (associated with AABW formation, AMOC, and IPO) likely contribute to hiatus and accelerated warming decades, here we focus on one of those, the IPO, to illustrate the interaction of internally generated variability and the externally forced response in the Pacific. The same methodology is applied as in Meehl et al. (2009) to the hiatus and accelerated warming decades in the RCP4.5 simulations of CCSM4.

Figure 5 (top) shows the first EOF of low-pass filtered (13-yr cutoff) Pacific SSTs from the multicentury CCSM4 preindustrial control run. This is the usual way that the IPO is defined (e.g., Meehl and Hu 2006). As for the PCM in Meehl et al. (2009), the familiar IPO pattern is the leading mode of unforced decadal time scale variability over the Pacific domain, explaining 33.9% of the variance for that region. To quantify the forced patterns, Figs. 5 (middle) and 5 (bottom) show the first and second EOFs, respectively, of the low-pass filtered ensemble average RCP4.5 runs with CCSM4 for the years 2006–2100. By computing the average of the five ensemble members, the presumption is that most of the signal is from the external forcing, having averaged out much of the internally generated climate variability. The associated principal component (PC) time series (not shown) also shares characteristics with the PCM results in Meehl et al. (2009), with the dominant EOF1 (Fig. 5b) explaining 94.5% of the variance being mostly the trend and EOF2, with 2.2% of the variance, representing an IPO-like pattern. In fact, the pattern correlation of the forced EOF2 in Fig. 5 (bottom) with the internally generated IPO in Fig. 5 (top) is +0.73, confirming the result from the earlier PCM model that the internally generated variability associated with the IPO is not totally independent from at least some component of the externally forced response. This leads us to apply the same method used by Meehl et al. (2009) to infer the relative contributions of the three patterns in Fig. 5 to hiatus and accelerated warming decades.

Figure 6 shows, for the five CCSM4 RCP4.5 ensemble members with the eight hiatus decades highlighted in gray, the pattern correlation time series for each of the three patterns in Fig. 5 projected onto the SSTs in each of the ensemble members. This is similar to what was

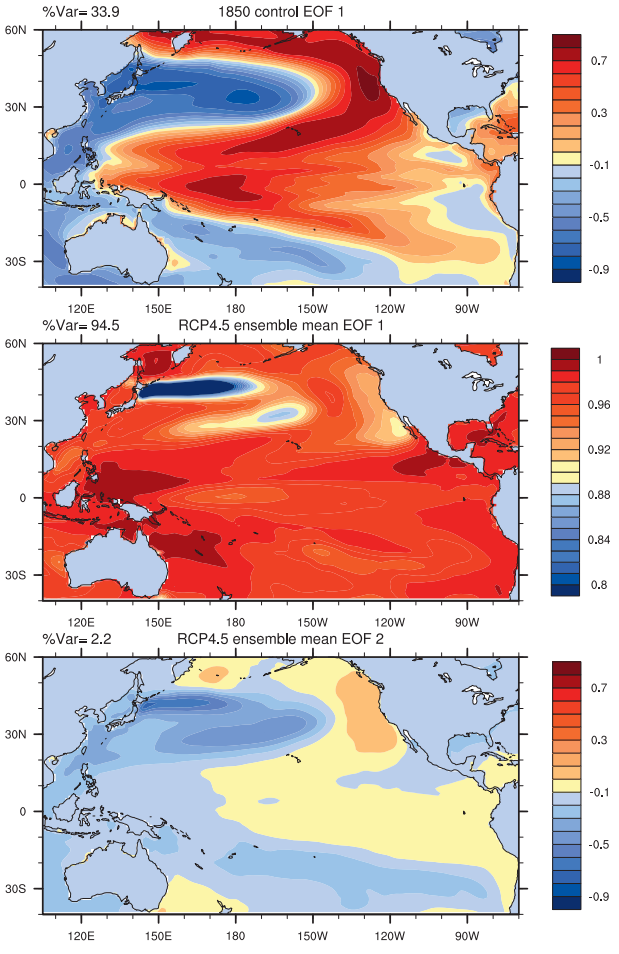

FIG. 5. (top) The first EOF of 13-yr low-pass filtered SSTs for the Pacific Ocean domain shown from a 300-yr period of the unforced CCSM4 control run (the model IPO). (middle) The first EOF of 13-yr low-pass-filtered SSTs for the ensemble mean RCP4.5 simulations from CCSM4 indicating the dominant forced response pattern. (bottom) As in the middle panel but for the second EOF.

done in Meehl et al. (2009) and involves taking each pattern in Fig. 5 and performing pattern correlations between those patterns and the annual mean patterns of SSTs in each of the ensemble members. The first feature of Fig. 6 is that the three pattern correlation time series are related and roughly track each other. This illustrates the interplay between the internally generated and externally forced patterns in the RCP4.5 simulations. Examination of the eight hiatus decades shows that in seven out of eight, there is a transition from positive to negative IPO (or less positive) and, correspondingly, less forced warming (mostly negative trends for those time periods). In the decade when the IPO shows the opposite transition, there is a weakening of the AMOC and AABW formation (not shown), thus indicating, as discussed in Fig. 3, that these other processes also contribute to the globally averaged signal. However in most

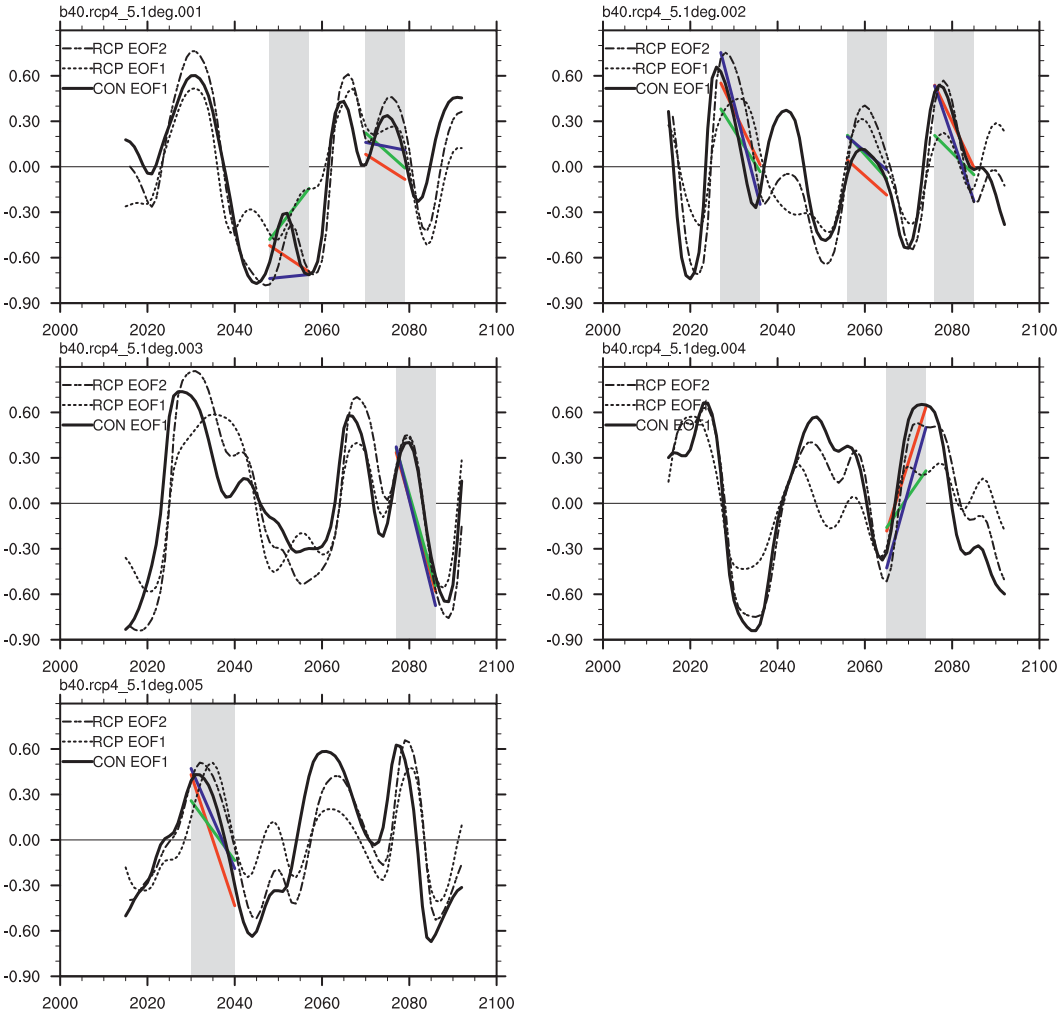

FIG. 6. Time series of pattern correlations from projecting the first EOF from the control run (the model IPO in Fig. 5, top) onto the low-pass filtered SST data from the five ensemble members of RCP4.5 from CCSM4 (solid lines); similarly, pattern correlations from projecting the first (dotted) and second (dashed) EOFs from the ensemble mean RCP4.5 experiments (middle and bottom panels of Fig. 5, respectively) onto the low-pass filtered SST data from the five ensemble members of RCP4.5 are also shown. Gray shading indicates the eight hiatus decades. Linear trend lines of the pattern correlation time series, within the gray-shaded periods, are plotted for the IPO (red) and EOF1 (green) and EOF2 (blue) of the ensemble average RCP4.5 simulations.

cases, as the tropical Pacific SSTs transition to negative anomalies with the IPO, there is less power in the positive SST trends from the forced patterns. In other words, the IPO tends to overcome the tendency for the tropical Pacific SSTs to warm from external forcing and produces negative SST trends there (Fig. 1a).

Figure 7 is a similar plot to Fig. 6, but highlights the seven accelerated warming decades. Figure 7 shows that six out of seven accelerated warming decades show a transition from negative to positive IPO (or less negative) and, correspondingly, more forced warming (mostly positive trends). For the one IPO transition early in ensemble member 2 that goes opposite to the others, there is a strengthening of AABW formation of over 10% (not shown) that produces the dominant contribution of the three processes discussed above to that accelerated warming decade. As noted earlier, any of the three processes (AABW formation, AMOC, or IPO) can make a contribution to either a hiatus or accelerated warming decade. But of the three, the IPO in the Pacific, interacting with the response to external forcing, is more consistent in contributing to those globally averaged signals.

A more detailed depiction of the SST signatures of the IPO, AABW, and AMOC is shown in Fig. 8. Indices for AMOC and AABW, as well as the PC time series of EOF1 from the control run that represents the IPO, are

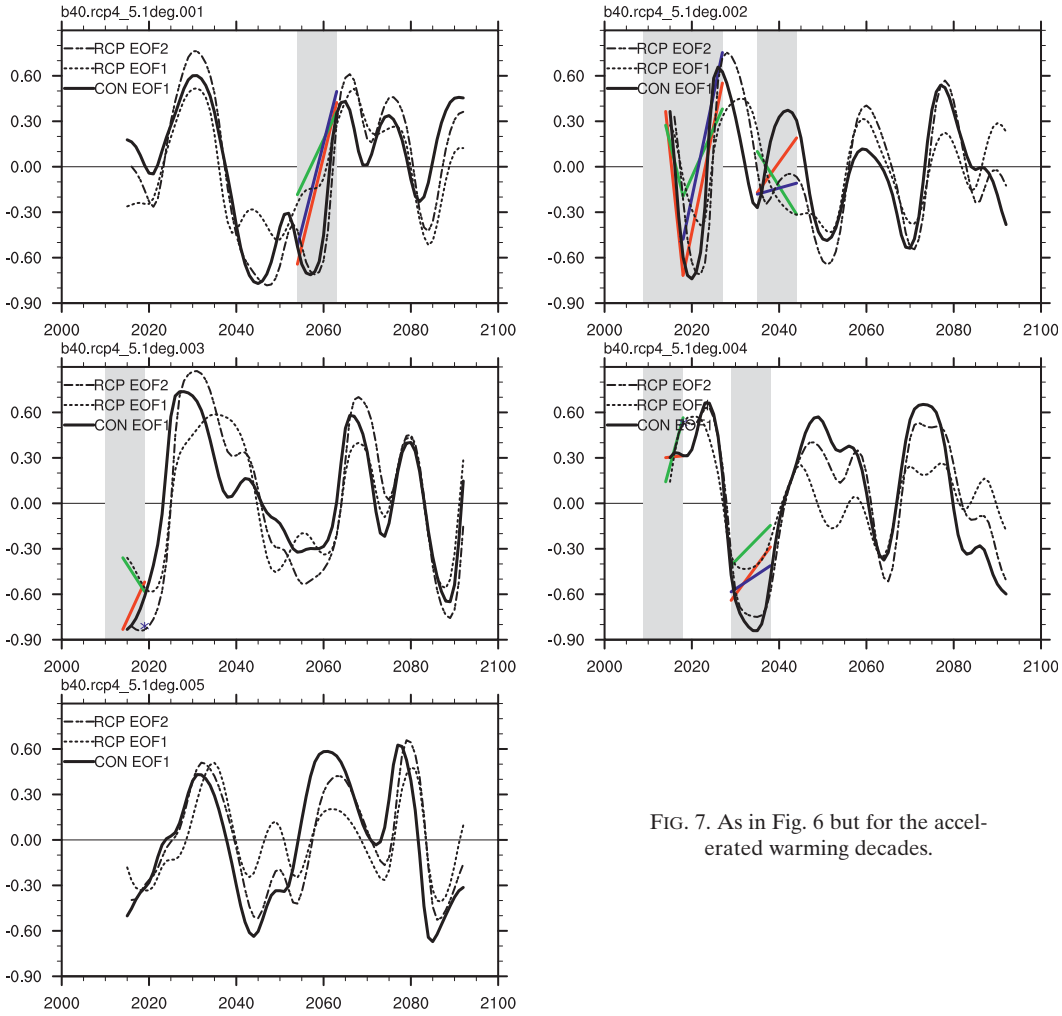

FIG. 7. As in Fig. 6 but for the accelerated warming decades.

regressed onto SSTs from the 300-yr control run [since there is no externally forced trend in the control run, EOF1 is the IPO, as opposed to EOF2 in the forced runs, where EOF1 is the externally forced trend (see Meehl et al. 2009)]. Use of the control run ensures that variability is only internally generated without any changes in external forcing.

The AMOC index is defined as the maximum of the meridional overturning streamfunction below 500-m depth in the Atlantic. The AABW index is defined as the minimum of the global meridional streamfunction between 60° and 80°S (for the regressions, the sign of the AABW index is reversed such that stronger AABW formation is a larger positive number).

The regression patterns in Fig. 8 show that the positive phase of the IPO (Fig. 8, top), a strong AMOC (Fig. 8, middle), and a strong AABW formation (Fig. 8, bottom) all exhibit similar SST patterns in the Pacific that resemble the positive phase of the IPO. Thus, the three processes all can contribute to a pattern with an IPO signature in the Pacific, though there are some interesting regional differences. Stronger AMOC is associated with a narrower band of positive SST anomalies in the equatorial Pacific than the other two, possibly linked with processes in the Atlantic described by Hu et al. (2013). In any case, it can be seen that any of the three processes can contribute to a similar large-scale SST anomaly pattern in the Pacific that can then interact with the externally forced response, as described above. The processes are thus not independent, which means that they are physically related and can work in various combinations to produce similar responses for hiatus and accelerated warming decades.

5. Conclusions

Previous studies have shown that globally averaged surface air temperature trends in some decades show little warming trend (termed hiatus decades, e.g., the

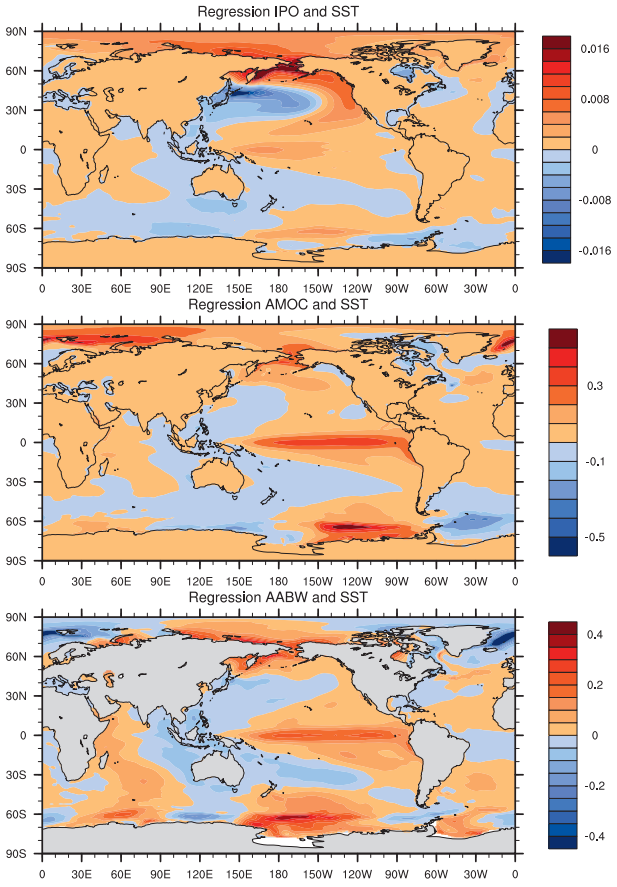

FIG. 8. Regression of indices of (top) IPO, (middle) AMOC, and (bottom) AABW on annual mean SSTs from the CCSM4 300-yr control run.

early 2000s), while others are characterized by a rapid increase of temperatures (termed accelerated warming decades, e.g., the 1970s). Here it is shown that such decades, seen in observations, are common in future climate simulations with a global coupled climate model (CCSM4) and are a natural product of interactions of internally generated decadal climate variability and external forcing. A five member ensemble from the RCP4.5 simulations with CCSM4 is analyzed to study the relative roles of internal variability and external forcing to hiatus and accelerated warming decades. The net energy imbalance at the top of the atmosphere is about $1\ \mathrm{W\,m^{-2}}$ during all decades considered, including the hiatus and accelerated warming decades. This indicates that the increase in GHGs in RCP4.5 is maintaining a fairly steady decadal net energy imbalance with excess heat being trapped in the system.

From the five ensemble members, a total of eight hiatus decades and seven accelerated warming decades were chosen. Hiatus periods of longer duration (up to 15 yr for a zero globally averaged temperature trend) also occur in the RCP4.5 simulations, suggesting that the current observed hiatus could continue for several more years.

Composite linear trends of SSTs show roughly opposite patterns, with greater cooling (warming) in the tropics and the tropical Pacific in particular, with the latter characterized by a negative (positive) phase of the interdecadal Pacific oscillation (IPO) in the hiatus (accelerated warming) decades. Analysis of heat content trends also shows opposite signals, with the upper 300 m of the global oceans warming less than the deeper ocean layers in the hiatus decades but with more rapid warming of the upper 300 m in the accelerated warming decades compared to the deeper ocean layers. Zonal mean meridional overturning streamfunction and temperature trends show that for the accelerated warming decades, there are weaker subtropical cells (STCs) in the Pacific with stronger Atlantic meridional overturning circulation (AMOC) and AABW formation, opposite to what is seen in the hiatus decades.

Analysis of each of the hiatus and accelerated warming decades shows that such decades can have contributions from AABW formation, AMOC, or STCs associated with the IPO either by themselves or in combination with the others. Indeed, all have global SST signatures similar to the IPO, demonstrating that they are not independent. However, of the three processes, the STCs associated with the IPO have the most consistent contribution to the hiatus and accelerated warming decades.

Results shown here are examples of the interplay in the Pacific between external forcing and internally generated decadal climate variability from the IPO. The warming from external forcing adds to the positive phase of the internally generated IPO to contribute to the decades characterized by accelerated warming, while cooling in the tropical Pacific from the negative phase of the IPO overcomes the warming from external forcing and thus contributes to hiatus decades. Each of the three internally generated processes can produce a similar SST anomaly pattern in the Pacific that can then interact with the externally forced response to contribute to hiatus or accelerated warming decades.

Acknowledgments. The authors thank Claudia Tebaldi for consultation on the statistical significance calculations and Jing-Jia Luo, Michael McPhaden, and three anonymous reviewers for constructive and helpful comments. Portions of this study were supported by the Office of Science (BER), U.S. Department of Energy; the National Science Foundation; and NASA Grant NNX09AH89G.

The CCSM project is supported by the National Science Foundation and the Office of Science (BER) of the U.S. Department of Energy. Computing resources were provided by the Climate Simulation Laboratory at NCAR's

Computational and Information Systems Laboratory (CISL), sponsored by the National Science Foundation and other agencies, as well as computing resources of the National Energy Research Scientific Computing Center and the Oak Ridge Leadership Computing Facility, both supported by the Office of Science (BER) of the U.S. Department of Energy. An award of computer time was provided by the Innovative and Novel Computational Impact on Theory and Experiment (INCITE) program.

REFERENCES

Balmaseda, M. A., K. E. Trenberth, and E. Källén, 2013: Distinctive climate signals in reanalysis of global ocean heat content. *Geophys. Res. Lett.,* **40,** 1754–1759, doi:10.1002/grl.50382.

Brady, E. C., and B. L. Otto-Bliesner, 2011: The role of meltwater-induced subsurface ocean warming in regulating the Atlantic meridional overturning in glacial climate simulations. *Climate Dyn.,* **37,** 1517–1532, doi:10.1007/s00382-010-0925-9.

Burgman, R. J., A. C. Clement, C. M. Mitas, J. Chen, and K. Esslinger, 2008: Evidence for atmospheric variability over the Pacific on decadal timescales. *Geophys. Res. Lett.,* **35,** L01704, doi:10.1029/2007GL031830.

Chen, J., A. D. Del Genio, B. E. Carlson, and M. G. Bosilovich, 2008: The spatiotemporal structure of twentieth-century climate variations in observations and reanalyses. Part II: Pacific pan-decadal variability. *J. Climate,* **21,** 2634–2650.

Dai, A., 2013: The influence of the inter-decadal Pacific oscillation on US precipitation during 1923–2010. *Climate Dyn.,* doi:10.1007/s00382-012-1446-5, in press.

Easterling, D. R., and M. F. Wehner, 2009: Is the climate warming or cooling? *Geophys. Res. Lett.,* **36,** L08706, doi:10.1029/2009GL037810.

Feng, M., M. J. McPhaden, and T. Lee, 2010: Decadal variability of the Pacific subtropical cells and their influence on the southeast Indian Ocean. *Geophys. Res. Lett.,* **37,** L09606, doi:10.1029/2010GL042796.

Gent, P. R., and Coauthors, 2011: The Community Climate System Model Version 4. *J. Climate,* **24,** 4973–4991.

Guemas, V., F. J. Doblas-Reyes, I. Andreu-Burillo, and M. Asif, 2013: Retrospective prediction of the global warming slowdown in the past decade. *Nat. Climate Change,* **3,** 649–653, doi:10.1038/nclimate1863.

Hansen, J., and Coauthors, 2005: Earth's energy imbalance: Confirmation and implications. *Science,* **308,** 1431–1435.

Hu, A., G. A. Meehl, W. Han, J. Yin, B. Wu, and M. Kimoto, 2013: Influence of continental ice retreat on future global climate. *J. Climate,* **26,** 3087–3111.

Katsman, C. A., and G. J. van Oldenborgh, 2011: Tracing the upper ocean's ''missing heat.'' *Geophys. Res. Lett.,* **38,** L14610, doi:10.1029/2011GL048417.

Klinger, B. A., and J. Marotzke, 2000: Meridional heat transport by the subtropical cell. *J. Phys. Oceanogr.,* **30,** 696–705.

Knight, J., and Coauthors, 2009: Do global temperature trends over the last decade falsify climate predictions? [in ''State of the Climate in 2009'']. *Bull. Amer. Meteor. Soc.,* **90,** S20–S21.

Levitus, S., J. I. Antonov, T. P. Boyer, R. A. Locarnini, H. E. Garcia, and A. V. Mishonov, 2009: Global ocean heat content 1955–2008 in light of recently revealed instrumentation problems. *Geophys. Res. Lett.,* **36,** L07608, doi:10.1029/2008GL037155.

——, and Coauthors, 2012: World ocean heat content and thermosteric sea level change (0–2000 m), 1955–2010. *Geophys. Res. Lett.,* **39,** L10603, doi:10.1029/2012GL051106.

Loeb, N. G., and Coauthors, 2012: Observed changes in top-of-the-atmosphere radiation and upper-ocean heating consistent within uncertainty. *Nat. Geosci.,* **5,** 110–113, doi:10.1038/ngeo1375.

Lyman, J. M., and Coauthors, 2010: Robust warming of the global upper ocean. *Nature,* **465,** 334–337, doi:10.1038/nature09043.

McPhaden, M. J., and D. Zhang, 2002: Slowdown of the meridional overturning circulation in the upper Pacific Ocean. *Nature,* **415,** 603–608.

——, and ——, 2004: Pacific Ocean circulation rebounds. *Geophys. Res. Lett.,* **31,** L18301, doi:10.1029/2004GL020727.

Meehl, G. A., and A. Hu, 2006: Megadroughts in the Indian monsoon region and southwest North America and a mechanism for associated multi-decadal Pacific sea surface temperature anomalies. *J. Climate,* **19,** 1605–1623.

——, and J. M. Arblaster, 2011: Decadal variability of Asian–Australian monsoon–ENSO–TBO relationships. *J. Climate,* **24,** 4925–4940.

——, and ——, 2012: Relating the strength of the tropospheric biennial oscillation (TBO) to the phase of the Interdecadal Pacific Oscillation (IPO). *Geophys. Res. Lett.,* **39,** L20716, doi:10.1029/2012GL053386.

——, W. M. Washington, C. Amman, J. M. Arblaster, T. M. L. Wigley, and C. Tebaldi, 2004: Combinations of natural and anthropogenic forcings in twentieth-century climate. *J. Climate,* **17,** 3721–3727.

——, A. Hu, and B. D. Santer, 2009: The mid-1970s climate shift in the Pacific and the relative roles of forced versus inherent decadal variability. *J. Climate,* **22,** 780–792.

——, ——, and C. Tebaldi, 2010: Decadal prediction in the Pacific region. *J. Climate,* **23,** 2959–2973.

——, J. M. Arblaster, J. Fasullo, A. Hu, and K. E. Trenberth, 2011: Model-based evidence of deep ocean heat uptake during surface temperature hiatus periods. *Nat. Climate Change,* **1,** 360–364, doi:10.1038/nclimate1229.

——, and Coauthors, 2012: Climate system response to external forcings and climate change projections in CCSM4. *J. Climate,* **25,** 3661–3683.

Palmer, M. D., D. J. McNeall, and N. J. Dunstone, 2011: Importance of the deep ocean for estimating decadal changes in Earth's radiation. *Geophys. Res. Lett.,* **38,** L13707, doi:10.1029/2011GL047835.

Power, S., T. Casey, C. Folland, A. Colman, and V. Mehta, 1999: Interdecadal modulation of the impact of ENSO on Australia. *Climate Dyn.,* **15,** 319–324.

Purkey, S. G., and G. C. Johnson, 2010: Warming of global abyssal and deep Southern Ocean waters between the 1990s and 2000s: Contributions to global heat and sea level rise budgets. *J. Climate,* **23,** 6336–6351.

Santer, B. D., and Coauthors, 2011: Separating signal and noise in atmospheric temperature changes: The importance of timescale. *J. Geophys. Res.,* **116,** D22105, doi:10.1029/2011JD016263.

Song, Y. T., and F. Colberg, 2011: Deep ocean warming assessed from altimeters, gravity recovery and climate experiment, in situ measurements, and a non-Boussinesq ocean general circulation model. *J. Geophys. Res.,* **116,** C02020, doi:10.1029/2010JC006601.

Trenberth, K. E., 2009: An imperative for climate change planning: Tracking Earth's global energy. *Curr. Opin. Environ. Sustainability,* **1,** 19–27.

——, and J. W. Hurrell, 1994: Decadal atmosphere-ocean variations in the Pacific. *Climate Dyn.,* **9,** 303–319.

——, and J. T. Fasullo, 2009: Global warming due to increasing absorbed solar radiation. *Geophys. Res. Lett.,* **36,** L07706, doi:10.1029/2009GL037527.

——, and ——, 2010: Tracking Earth's energy. *Science,* **328,** 316–317.

——, ——, and J. Kiehl, 2009: Earth's global energy budget. *Bull. Amer. Meteor. Soc.,* **90,** 311–323.

Wang, B., and S.-I. An, 2001: Why the properties of El Niño changed during the late 1970s. *Geophys. Res. Lett.,* **28,** 3709–3712.

Watanabe, M., Y. Kamae, M. Yoshimori, A. Oka, M. Sato, M. Ishii, T. Mochizuki, and M. Kimoto, 2013: Strengthening of ocean heat uptake efficiency associated with the recent climate hiatus. *Geophys. Res. Lett.,* **40,** doi:10.1002/grl.50541, in press.